ACS Sustainable Chemistry & Engineering

Research Article

pubs.acs.org/journal/ascecg

Preparation of Nano- and Microstructured Garnet $Li_7La_3Zr_2O_{12}$ Solid Electrolytes for Li-Ion Batteries via Cellulose Templating

Zachary D. Gordon,[†] Ting Yang,[‡] Guilherme Bruno Gomes Morgado,[‡,§] and Candace K. Chan*[,‡]

[†]Chemical Engineering and [‡]Materials Science and Engineering, School for Engineering of Matter, Transport and Energy, Arizona State University, 501 East Tyler Mall ECG 301, Tempe, Arizona 85287, United States

[§]Institute of Mecânica Engineering (Instituto de Engenharia Mechanica), Federal University of Itajubá (Universidade Federal de Itajubá), 1303 BPS Avenue, Pinheirinho, Itajubá, Minas Gerais 37500-903, Brazil

Supporting Information

ABSTRACT: Lithium lanthanum zirconate (LLZO) is a promising Li^+ ion conductor for applications as a ceramic solid electrolyte in all-solid-state lithium batteries. However, the tetragonal and cubic phases of LLZO differ in lithium ionic conductivity by several orders of magnitude with extrinsic dopants or nanostructuring often required to stabilize the high conductivity cubic phase at room temperature. Here, we show that nanostructured LLZO can be prepared by templating onto various cellulosic fibers, including laboratory Kimwipes, Whatman filter paper, and nanocellulose fibrils, followed by calcination at 700−800 °C. The effect of templating material, calcination temperature, calcination time, and heating ramp rate on the LLZO crystal structure and morphology were thoroughly investigated. Templating was determined to be an effective method for controlling the LLZO size and morphology, and low calcination times and ramp rates were found to favor the formation of small ligaments. Furthermore, it was verified that cubic phase stabilization occurred for LLZO with ligaments of size less than 1 μm on average without the use of extrinsic dopants. This work provides more information regarding the size dependence of cubic LLZO stabilization that was not previously investigated in detail, and cellulosic templating is shown to be a viable route toward the scalable, sustainable synthesis of LLZO solid electrolytes.

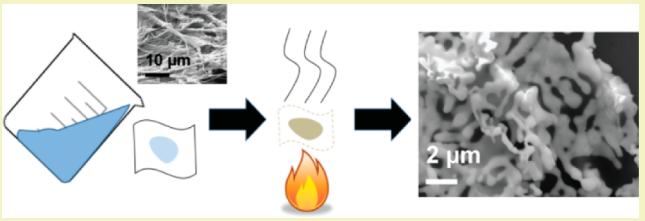

KEYWORDS: *Li-ion batteries, Solid electrolyte, Lithium lanthanum zirconate, Nanocellulose, Templating*

INTRODUCTION

Lithium-ion batteries are the predominant means for electrical energy storage in most portable electronics applications, including hybrid/electric vehicles, laptops, and cellular phones. However, these batteries pose safety concerns due to their flammability and tendency to ignite upon short-circuiting or overcharging. The development of solid electrolytes that can improve the safety characteristics of lithium batteries through elimination of the organic electrolyte is an increasingly active research area.

Recently, garnet-type solid Li^+ ion conductors such as $Li_7La_3Zr_2O_{12}$ (LLZO) have received much attention as ceramic electrolytes for all-solid-state lithium batteries due to several favorable properties such as high stability to lithium[1] and ionic conductivity up to 10^{-3}−10^{-4} S/cm when prepared in the cubic phase (c-LLZO, space group: $Ia\bar{3}d$).[1,2] However, the thermodynamically stable tetragonal phase (t-LLZO, space group: $I4_1/acd$) typically displays 2 orders of magnitude lower ionic conductivity than that of c-LLZO.[3] The structural properties of c-LLZO and t-LLZO (Figure 1) account for the large difference in ionic conductivity between the two phases; c-LLZO exhibits delocalization of lithium atoms,[4] partially occupied Li sites, and a greater concentration of lithium vacancy defects.[5] The stabilization of c-LLZO at room temperature can be readily achieved through extrinsic doping (e.g., Al, Ta, Nb, or Ga).[4,6−8] Aluminum doping, however, possesses issues including the formation of the byproduct $LaAlO_3$, which limits the overall ionic conductivity,[4,9] and greater activation energy for Li^+ conduction, likely due to the electrostatic repulsion of Al^{3+} ions in Li^+ sites and limited lithium ion mobility.[10]

As an alternative to extrinsic doping, we have recently discovered a size-dependence in the phase stability of LLZO that could potentially be exploited. Nanostructured LLZO, either synthesized in a bottom-up approach via electrospinning or prepared in a top-down fashion by particle-size reduction of bulk powders using ball milling, was observed to remain stable as c-LLZO at room temperature without the use of dopants.[11] Our findings indicated that c-LLZO formed as interconnected "ligaments" with dimensions of 100−200 nm after the electrospun polymer fibers containing LLZO sol−gel precursor were calcined at 700 °C for 2.5−3 h. At longer heating times, the ligaments coalesced to form larger micrometer-sized

Received: May 11, 2016
Revised: August 10, 2016
Published: October 3, 2016

ACS Publications © 2016 American Chemical Society

DOI: 10.1021/acssuschemeng.6b01032
ACS Sustainable Chem. Eng. 2016, 4, 6391−6398

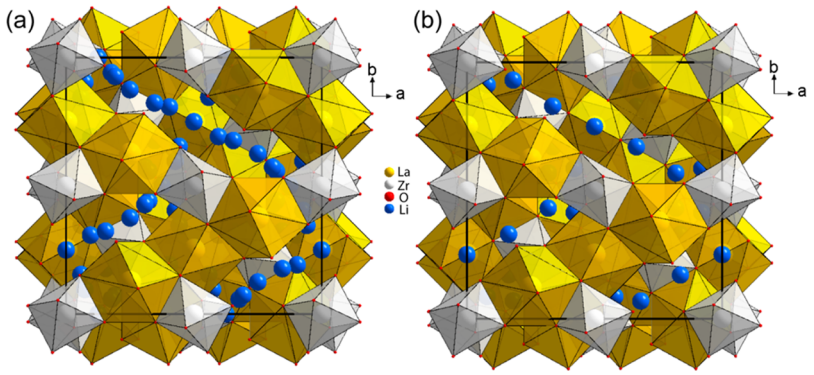

Figure 1. Crystal structure of (a) c-LLZO and (b) t-LLZO; yellow dodecahedra correspond to LaO_8 and white octahedra correspond to ZrO_6. There is clear evidence of Li ion clustering and disorder in c-LLZO compared to that in t-LLZO.

particles with t-LLZO structure, strongly pointing to a direct relationship between particle size and phase stability.[11]

As a preliminary hypothesis, we predict that there is a critical size below which the cubic phase is stabilized, which we have further validated herein through a novel synthesis of nanostructured c-LLZO via templating onto cellulose substrates, including nanocellulose. Cellulosic templating is an effective technique for synthesizing metal oxide films in porous morphologies.[12−14] To template ceramics, the cellulose substrate is typically impregnated with a sol−gel containing the ceramic precursor, which is subsequently combusted to remove the organic materials and calcined to obtain the ceramic in the desired crystal structure and morphology. The pore structure and size of the ceramic are largely influenced by the structure and porosity of the original template material.[15] For example, material templated on nanostructured fibers will result in a high surface area nanostructured replicate.[16] Typical cellulose polymers found in plant cell walls are composed of nanoscaled fibers of diameter 2−20 nm, known as nanocellulose fibrils (NCF).[17] Recently, methods including mechanical processes (high-pressure homogenization, ultrasonic treatments, cryocrushing), acid or enzymatic hydrolysis, and electrospinning have been developed for the preparation or extraction of NCF from cellulose.[17−19] NCF can be obtained in bulk quantities in an aqueous suspension, freeze- or spray-dried forms, or as nanocrystals.[20] NCF has been investigated as a renewable and sustainable approach to nanomaterial synthesis across many different green applications,[21] such as hydrogels for drug delivery and tissue engineering,[22] aerogel and hydrogel absorbents for oil and solvent cleanup,[23,24] reinforcements for transparent composites in defense applications,[25] and nanopaper substrates in flexible organic electronics.[26]

The investigation of cellulose fibers as a template is an extension of our previous work on electrospun LLZO materials in which the organic and polymeric precursors were removed during calcination, leaving the crystalline ceramic with nanostructured dimensions. By using different forms of cellulose as a template, the role of fiber size on the dimensions of the resulting ceramic can be studied, which can enable better understanding of the critical dimensions required for obtaining c-LLZO in the absence of extrinsic dopants. Hence, templating on nanocellulose fibrils is expected to produce LLZO with smaller dimensions compared to materials prepared using conventional cellulose templates. To the best of our knowledge, templating approaches have not been previously used in LLZO synthesis to control the particle size and crystal structure. A viable, scalable method of producing high-conductivity LLZO would enable its application as an electrolyte in solid-state batteries, thereby eliminating the flammable safety hazard inherent in current lithium batteries.

Here, we demonstrate that LLZO with ligament morphology can be prepared through cellulosic templating of sol−gel precursor followed by calcination. Two types of papers (Whatman filter paper and laboratory Kimwipes) and nanocellulose fibrils were investigated as templates. The effect of calcination temperature, heating time, and heating rate on the ligament size, surface area, and obtained LLZO crystal structure phase were studied.

EXPERIMENTAL SECTION

The nitrate-based LLZO sol precursor and nontemplated LLZO synthesis were prepared without extrinsic dopants such as Al^{3+} according to a sol−gel synthesis from Janani et al. with lithium nitrate, lanthanum nitrate, and zirconium(IV) oxynitrate precursors, citric acid as the complexing agent, and isopropyl alcohol as the solvent;[27] the detailed procedures can be found in the Supporting Information.

Nanocellulose fibrils (NCF) were obtained from the University of Maine Process Development Laboratory in both aqueous suspension (S-NCF) and spray-dried powder forms (D-NCF). For the NCF slurry to be used as a template, a sample of the raw material was dried in air to remove water before absorbing the LLZO precursor sol. For one experiment (W-NCF), LLZO sol was impregnated directly onto the as-received wet NCF slurry rather than air-drying it first. NCF was reported by the supplier to have 20 nm diameter fibrils. For comparison, commercial filter paper (Whatman 42) and laboratory task wipers (Kimwipes) were also investigated as cellulosic templates.

Templating was performed by placing the cellulose template in a glass dish and adding 10−15 mL of LLZO sol precursor to fully soak the template (Supporting Information). The saturated template was allowed to dry in air for several hours before undergoing heat treatment similar to that used in the nontemplated LLZO synthesis. Calcination was performed using an alumina crucible in a box furnace open to air. For certain experiments, a quartz crucible was used instead of alumina. Nontemplated LLZO was prepared by calcining the dried sol precursor directly using calcination at 800 °C for 12 h and 1 °C/min ramp rate in the absence of a cellulose template.

X-ray diffraction (XRD, PANalytical X'Pert Pro with Cu Kα radiation) was used for identification of the composition and phase of the resulting materials. For c-LLZO, there is one distinct peak at 2θ = 16° and three distinct peaks around 2θ = 51−54°. For t-LLZO, the 2θ = 16° peak splits into a peak doublet, and at 2θ = 51−54°, there are five groups of doublets/triplets. Scanning electron microscopy (SEM, FEI XL30 at 10 kV) was used to observe the morphology, and Brunauer−Emmett−Teller (BET, Micromeritics Tristar II) surface area measurements were performed. A transmission electron

DOI: 10.1021/acssuschemeng.6b01032
ACS Sustainable Chem. Eng. 2016, 4, 6391−6398

microscopy (TEM) study was carried out on a JEOL 2010F microscope at 200 kV.

RESULTS AND DISCUSSION

SEM images of the original cellulosic templates are shown in Figure 2, providing an approximation of the starting fiber

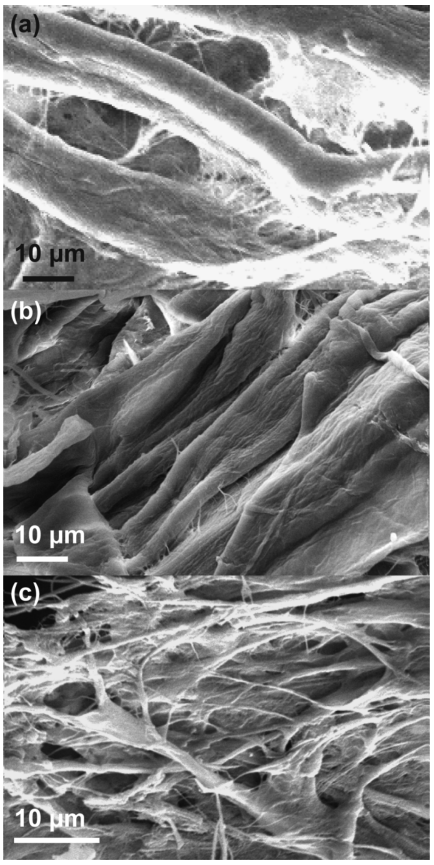

Figure 2. SEM images of template material before LLZO sol impregnation for (a) Whatman 42, (b) Kimwipes, and (c) NCF slurry dried in air.

diameter before LLZO sol impregnation and heat treatment. The pore size and porosity of Whatman 42 filter paper is 2.5 μm and 100 g/m^2, respectively, as reported by the vendor (Sigma-Aldrich); from Figure 2b, the pore size of Kimwipes is estimated to be of similar magnitude to Whatman 42 filter paper. The nanocellulose fibrils were reported to be 20 nm in diameter from the supplier, but in Figure 2c, the smallest fibers are approximately 100−200 nm in diameter; it is likely that the fibers in the SEM image are actually composed of thinner ∼20 nm fibers, which cannot be seen clearly at that magnification.

Figure 3a shows the SEM image for the nontemplated LLZO, which consisted of conglomerates of solid bulk particles between 10 and 20 μm in size. In contrast, SEM imaging revealed that using cellulose templates resulted in LLZO with microstructures resembling interconnected "ligaments" separated by pores or voids. The average ligament size was determined by obtaining diameter measurements along the length of each ligament observed in the SEM image and taking the average of all the measurements. Representative SEM images for LLZO templated onto NCF, Kimwipes, and Whatman 42 filter paper are shown in Figure 3b−d, respectively, after calcination at 800 °C for 12 h using a 1

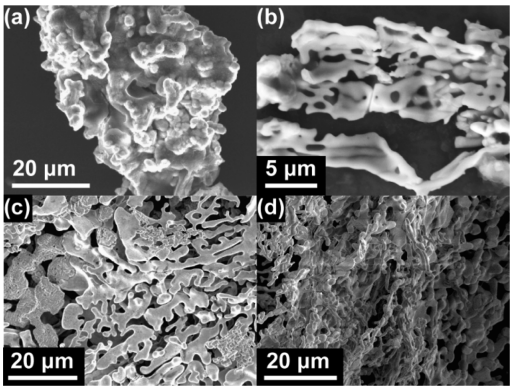

Figure 3. SEM images of LLZO annealed at 800 °C for 12 h and 1 °C/min ramp rate for (a) nontemplated materials (t-LLZO) and materials templated on (b) nanocellulose fibrils (c-LLZO), (c) Kimwipes (t-LLZO), and (d) Whatman 42 filter paper (t-LLZO).

°C/min ramp rate. As expected, materials obtained using Kimwipe and Whatman 42 templates exhibited larger fiber networks compared to those from the NCF template, validating that templating on NCF produces smaller LLZO fibrils.

The corresponding XRD patterns for these samples are shown in Figure 4. XRD analysis of the products indicated that,

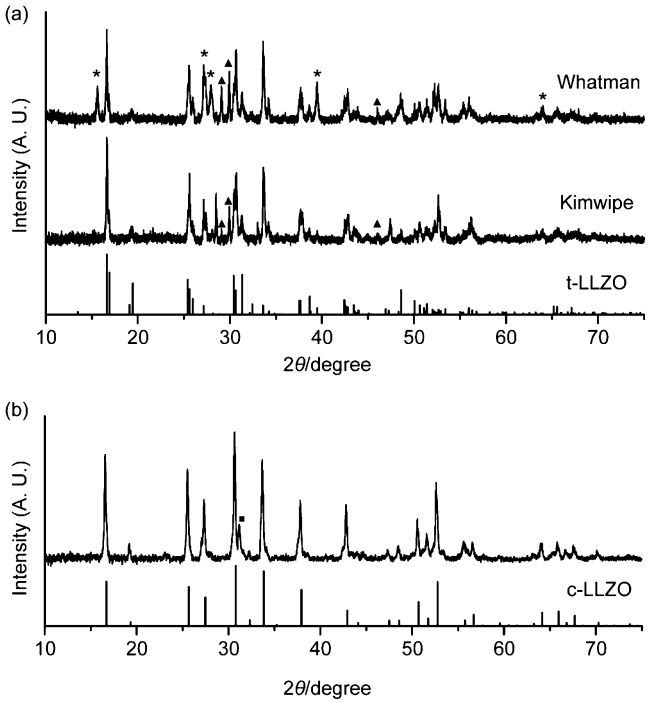

Figure 4. XRD plots of LLZO templated on different cellulose templates followed by calcination at 800 °C for 12 h with 1 °C/min ramp rate. (a) Whatman 42 and Kimwipe templates resulted in t-LLZO; (b) NCF template resulted in c-LLZO (run N1). (*) $La(OH)_3$; (▰) La_2O_3; (○) $La_2Zr_2O_7$; (■) unidentified impurity.

using these conditions, the Whatman 42 and Kimwipe templates both produced t-LLZO (with secondary phases such as $La(OH)_3$, La_2O_3, and $La_2Zr_2O_7$), whereas using NCF resulted in c-LLZO with notably fewer impurities. The XRD pattern of the LLZO sol−gel calcined without use of a template (i.e., nontemplated LLZO) at the same conditions revealed the formation of t-LLZO (Figure S1). These results show the role

DOI: 10.1021/acssuschemeng.6b01032
ACS Sustainable Chem. Eng. 2016, 4, 6391−6398

of the template in affecting the formation of t-LLZO vs c-LLZO with the smaller fiber template favoring c-LLZO over large fiber templates or no template. The average ligament size for the templated t-LLZO samples was measured to be between 2.0 and 2.5 μm compared to ~1.1 μm for the c-LLZO sample templated on NCF.

For the roles of calcination temperature, heating time, and heating rate on the ligament size and obtained LLZO phase to be better understood, a series of parametric studies were performed for LLZO templated on Kimwipes and Whatman 42 paper. The results are summarized in Table 1. Select SEM images and ligament size distributions are shown in Figure S2, and XRD patterns for all runs are shown in Figures S3 and S4. From these results, it is apparent that the annealing temperature has the most significant impact on ligament size and formation of c-LLZO. The c-LLZO phase was observed for both Kimwipe and Whatman templates when the calcination temperature was decreased to 700 °C; in these cases, the measured ligament size was below 1 μm, whereas conditions that produced t-LLZO had larger ligament sizes. Heating the nontemplated LLZO at 700 °C for 5 h resulted in the formation of t-LLZO with La_2O_3 impurities (Figure S1). These results show that the presence of the template will promote the formation of c-LLZO. There is also a general trend for templated samples to form smaller ligaments at lower heating rates; a ramp rate of 1 °C/min is favorable for small ligament formation, whereas faster heating rates result in thickening of ligaments and thus t-LLZO stabilization. The significance of heating time on the LLZO phase was not clear for these templating results, but it is expected that increased heating time induces coalescence of ligaments as shown in our previous research[11] in addition to improving the crystallinity. As an example, the XRD patterns for W6 and K6 (both calcined at 700 °C for 12 h) and W5 and K5 (both calcined at 700 °C for 24 h) are compared in Figure S5. It is clear that the longer calcination time for W5/K5 improved the crystallinity of the LLZO and decreased the number of impurities compared to those of W6/K6.

Table 1. Identified Phases and Ligament Size for Templating with Kimwipes (K-runs) and Whatman 42 (W-runs) under Different Calcination Conditions

run	temp. (°C)	heating time (h)	heating rate (°C/min)	phase	ligament size (μm)
K1	800	24	5	t-LLZO	2.41 ± 1.30
K2	800	12	5	t-LLZO, La_2O_3, $La_2Zr_2O_7$	2.57 ± 1.49
K3	800	24	1	t-LLZO, La_2O_3, $La_2Zr_2O_7$	1.73 ± 0.86
K4	800	12	1	t-LLZO, La_2O_3, $La_2Zr_2O_7$	2.46 ± 1.52
K5	700	24	5	c-LLZO, La_2O_3, $La_2Zr_2O_7$	1.09 ± 0.59
K6	700	12	5	t-LLZO, $La(OH)_3$, La_2O_3, $La_2Zr_2O_7$	1.45 ± 0.96
K7	700	24	1	c-LLZO, t-LLZO	0.95 ± 0.54
K8	700	12	1	c-LLZO, La_2O_3, $La_2Zr_2O_7$	0.93 ± 0.52
W1	800	24	5	t-LLZO, La_2O_3, $La_2Zr_2O_7$	1.43 ± 0.60
W2	800	12	5	t-LLZO, La_2O_3, $La_2Zr_2O_7$	1.62 ± 0.73
W3	800	24	1	La_2O_3, $La_2Zr_2O_7$	
W4	800	12	1	t-LLZO, La_2O_3, $La_2Zr_2O_7$	1.51 ± 0.80
W5	700	24	5	t-LLZO, $La(OH)_3$	1.21 ± 0.80
W6	700	12	5	t-LLZO, $La(OH)_3$	2.29 ± 1.25
W7	700	24	1	c-LLZO, $La(OH)_3$, $La_2Zr_2O_7$	0.89 ± 0.52
W8	700	12	1	c-LLZO, $La(OH)_3$, $La_2Zr_2O_7$	0.93 ± 0.46

The XRD analysis showed that the use of both Kimwipes and Whatman templates resulted in a number of impurities and secondary phases. The presence of $La(OH)_3$ in several runs was unexpected. It is speculated that the impurities formed from unreacted La^{3+} due to insufficient diffusion and reaction of precursors through the larger fibers and ligament dimensions in the microstructured templates. Additionally, we observed that $La(OH)_3$ impurities were less likely in sol−gels prepared with increased evaporation time and hence reduced water content. Fleming et al. previously demonstrated the rapid hydroxylation of the common LLZO byproduct La_2O_3 to $La(OH)_3$ when exposed to ambient conditions for as little as 8 h.[28] On the other hand, $La_2Zr_2O_7$ is a common intermediate compound in LLZO synthesis and indicates the incomplete formation of LLZO due to too low of a temperature, too short of a calcination time, or lithium loss,[2,27,29,30] which is consistent with our results here.

In general, templating onto Whatman 42 tended toward the formation of products with greater amounts of impurities and secondary phases compared to those obtained when using the Kimwipe templates, as shown in the XRD patterns in Figure S4. This could result from an interaction between La^{3+} and some component of the Whatman 42 fibers not found in the other templates. This speculation is evidenced by the experimental technique for Kimwipe and Whatman 42 templating experiments; the same batch of sol−gel precursor was used for both

Table 2. Identified Phases and Ligament Size for Templating with Nanocellulose Fibrils (NCF) after Different Calcination Conditions in Al_2O_3 Crucible[a]

run	template	temp. (°C)	heating time (h)	heating rate (°C/min)	composition	ligament size (μm)
N1	S-NCF	800	12	1	c-LLZO	1.11 ± 0.54
N2	S-NCF	700	24	1	c-LLZO, La_2O_3	0.53 ± 0.30
N3	D-NCF	700	24	1	c-LLZO, $La_2Zr_2O_7$, La_2O_3	0.95 ± 0.59
N4	S-NCF	700	6	2	c-LLZO, $La(OH)_3$ $La_2Zr_2O_7$	0.77 ± 0.40
N5.1	S-NCF	700	6	1	c-LLZO, La_2O_3	0.49 ± 0.24
N5.2	S-NCF	700	6	1	c-LLZO	0.84 ± 0.40
N6	W-NCF	700	6	1	c-LLZO, t-LLZO, $La_2Zr_2O_7$	1.39 ± 0.79
N7	S-NCF	700	3	1	$La_2Zr_2O_7$	

[a]S-NCF: dried slurry NCF; W-NCF: wet slurry NCF; D-NCF: dry NCF.

DOI: 10.1021/acssuschemeng.6b01032
ACS Sustainable Chem. Eng. 2016, 4, 6391−6398

templates, and Kimwipe and Whatman 42 experiments were performed simultaneously with identical heat treatments.

The composition and ligament size for templating experiments performed on NCF are shown in Table 2. Nanocellulose templating was more effective at obtaining c-LLZO with mean ligament size less than 500 nm with fewer impurities and secondary products than with the other templates. The smaller ligament size in the obtained LLZO correlates with the smaller diameter of the cellulose fibers in NCF (~20 nm) compared to the other templates, which had microstructured fibers. Hence, after absorption of LLZO sol by the NCF template and following calcination, the resulting ligament size should be consistent with the original template, though expanding in the heating process. The samples templated on the slurry form of NCF (S-NCF) did not have significant impurities, but the sample templated on dry NCF (run N3) yielded c-LLZO in addition to intermediate phase $La_2Zr_2O_7$, La_2O_3, and unidentified impurities, as illustrated in the XRD pattern in Figure S6a. For this reason, the slurry form of NCF was the template of choice for the NCF templating experiments due to the nontrivial amount of impurities formed with the dry NCF template.

The effect of calcination time on the formation of c-LLZO is shown in Figure 5 for templating on NCF at 700 °C. The c-

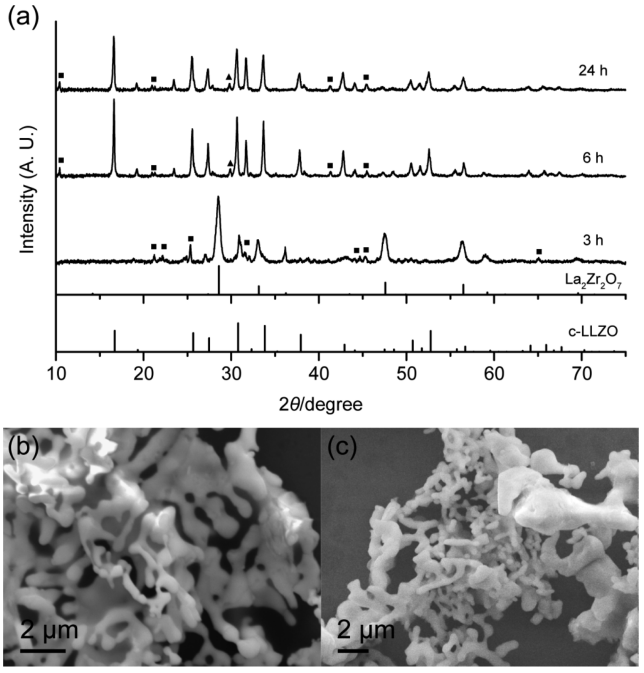

Figure 5. (a) XRD pattern of LLZO template on nanocellulose fibrils calcined for 3 h (run N7), 6 h (run N5.1), and 24 h (run N2) at 700 and 1 °C/min ramp rate in an alumina crucible; (▲) La_2O_3; (■) unidentified phase. SEM image of LLZO fibers after (b) 6 and (c) 24 h of calcination.

LLZO was successfully formed for heating times of 6 h and above with only small La_2O_3 impurities, whereas only $La_2Zr_2O_7$ and another unidentified phase were produced after 3 h of calcination. Hence, c-LLZO synthesis via NCF templating requires at least 6 h of calcination at 700 °C. Calcination longer than 6 h did not appear to have a significant impact on ligament size of c-LLZO formation, as shown in the SEM images in Figure 5b and c and the ligament size in Table 2. There are noticeably larger fibers in Figure 5c for the sample calcined for 24 h, but the average ligament size was nearly equal to that for the sample calcined for 6 h. It has been documented that calcination of LLZO precursor in an alumina crucible can result in diffusion of Al^{3+} into the sample to form Al-dopant-stabilized c-LLZO.[31,4,5] Performing identical heating experiments on the NCF templated LLZO in quartz crucibles showed products with similar composition (Figure S7) and ligament sizes as those calcined in alumina crucibles, confirming that our observed stabilization of c-LLZO at room temperature is not originating from inadvertent doping from Al^{3+}.

TEM characterization was performed on samples templated on NCF to characterize the structure of the c-LLZO (Figure 6a) and intermediate phases (Figure 6b–d). TEM observation

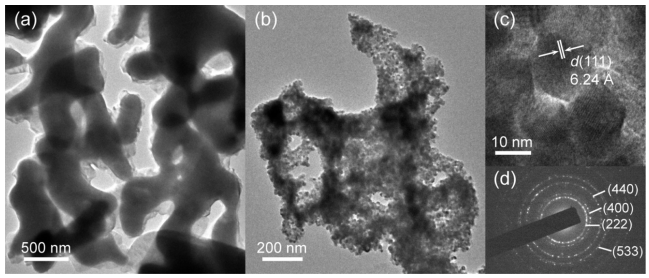

Figure 6. TEM image of (a) c-LLZO sample templated on NCF (Run N5.1) showing the ligaments and (b) $La_2Zr_2O_7$ sample templated on NCF (Run N7); (c) high-resolution TEM image of $La_2Zr_2O_7$ nanocrystals; (d) SAED pattern of the $La_2Zr_2O_7$ sample.

for samples calcined with insufficient heating time to form LLZO (run N7; 700 °C for 3 h) showed that the $La_2Zr_2O_7$ majority phase consisted of fine grains ranging from ~10–20 nm in size (Figure 6b and c). The selected area electron diffraction (SAED) pattern showed concentric rings corresponding to $La_2Zr_2O_7$ (Figure 6d). The corresponding XRD pattern (Figure 5a) also showed broadened peaks as a result of the small crystal sizes. This is consistent with our previous finding in electrospun LLZO nanowires that the primary crystalline phase is $La_2Zr_2O_7$ nanocrystals when the LLZO formation reaction is incomplete.[11]

TEM characterization was performed on c-LLZO obtained from run N5.1 (700 °C for 6 h). Unfortunately, the sample was very vulnerable to electron beam damage, and only low magnification images were taken. TEM examination showed that the morphology agrees with the observation from SEM and that the templated sample was made up of interconnected ligaments (Figure 6a). The TEM observation further revealed that each ligament was composed of multiple grains. Therefore, the ligament size is not necessarily equivalent to grain size, and most of the time the grain size is smaller than the ligament size with multiple grains found across the diameter of one ligament. Hence, measurement of the ligament sizes cannot provide the critical size below which the material will be stable as c-LLZO because this does not directly access the grain size information. However, because in general large grains are thermodynamically favored over small ones, the probability of growing large grains in thick ligaments is higher under the same conditions because there is less dimensional restriction. Development of synthesis methods for well-controlled LLZO (e.g., through a chemical synthesis route that can provide shape/size-controlled materials that are each a single crystal) may be able to shed more light on the precise transition size between t-LLZO and c-LLZO.

DOI: 10.1021/acssuschemeng.6b01032
ACS Sustainable Chem. Eng. 2016, 4, 6391–6398

Additionally, Table 3 provides a correlation between the ligament sizes measured in SEM and the BET surface area of the samples. Samples with smaller ligament size exhibited greater surface area, as expected. The information in Table 3 verifies that the method of ligament size measurement was effective at estimating particle size. Further, there is a correlation between the BET surface area and the preferred LLZO phase with c-LLZO observed in higher surface area samples. In run N6 templated on the wet NCF slurry without air-drying (W-NCF) and calcined at 700 °C, the product contained a mixture of t-LLZO and c-LLZO and surface area of 2.14 m^2/g, which is between the measured surface areas for samples containing t-LLZO (~0.4 m^2/g) and c-LLZO (~2.5 m^2/g). In the absence of a template or some other morphology-controlling medium, the LLZO particles will coalesce and adopt the thermodynamically stable structure during calcination, namely, the large particles of t-LLZO (i.e., the nontemplated materials shown in Figure 3a). However, if the amount of precursor available is restricted by the use of a cellulose template to absorb the reagents, the LLZO can form as small particles. The mechanism for the phase stability of c-LLZO at room temperature in nanostructured LLZO is still not completely understood. Because we observed that samples with smaller ligaments and high surface area favor the c-LLZO structure, we believe that there is a difference in surface energy between c-LLZO and t-LLZO that enables the size-dependent phase stabilization. Similar size dependent phase stabilization has been observed in titania and zirconia polymorphs,[32−38] so it is plausible that a similar occurrence could account for cubic stabilization of LLZO below critical size parameters.

Table 3. Comparison of Ligament Size, BET Surface Area, and LLZO Phase for Various Samples

sample	ligament size (μm)	BET (m^2/g)	phase
N5.2	0.84	2.72	c-LLZO
N4	0.77	2.47	c-LLZO, $La(OH_3)$, $La_2Zr_2O_7$
N6	1.39	2.14	c-LLZO, t-LLZO mixture
K4	2.46	0.35	t-LLZO
nontemplated	N/A	0.42	t-LLZO

In our experiments, we found that the calcination temperature of 700 °C is high enough to crystallize the LLZO precursor and remove the organic material. Heating at 800 °C tends to result in grain coalescence and the formation of larger ligaments, which prefer the t-LLZO phase. However, use of the NCF templates can facilitate the formation of smaller ligaments, which tend to form c-LLZO with fewer impurities and secondary phases than the other templates. Typical sintering temperatures to prepare dense pellets of LLZO suitable for use as solid electrolytes in lithium batteries are in the range of 1100−1230 °C,[2,39−41] which would preclude the use of the size-stabilized nanostructured c-LLZO because it would inevitably undergo grain coalescence and transform to t-LLZO under these conditions. However, advanced sintering techniques such as two-step sintering (TSS), spark plasma sintering (SPS), or templated grain growth sintering (TGGS) could potentially be employed to create dense pellets from c-LLZO nanostructures. Such methods have been previously utilized for preparing dense pellets of nanowires without grain growth.[42−45] The nanostructured c-LLZO could also be utilized as ceramic fillers in polymer electrolyte composites, which has recently been demonstrated to be a promising way to improve the Li^+ ionic conductivity of polymers such as polyacronitrile and poly(ethylene oxide).[46,47]

In summary, the experimental results indicate that templating is a viable option for nanostructured or microstructured LLZO synthesis. SEM images verify that LLZO ligaments produced using templating correlated to the size of the cellulose fibers in the original template material. By templating with nanocellulose, Whatman 42, or Kimwipes under appropriate calcination conditions, nanostructured c-LLZO could be synthesized, although the NCF template yielded the most phase-pure product. Additionally, cellulosic templating experiments elucidated the impact of lower calcination temperature and heating rate on reduced LLZO ligament size. By comparing the mean ligament size and BET surface area to LLZO phase, there is clear evidence that c-LLZO phase stabilization at room temperature occurs below critical ligament dimensions of ~1 μm, supporting previous results from electrospun LLZO[11] and showing that c-LLZO is generally formed in nanoscaled ligaments. As the annealing time is increased, the ligaments grow in size and revert back to t-LLZO, the thermodynamically preferred structure of bulk LLZO at room temperature. The use of cellulosic templating is a viable route toward the scalable, sustainable synthesis of nanostructured c-LLZO solid electrolytes, which is an important step for obtaining large quantities of materials for future studies focused on the evaluation of their ionic conductivity and performance in Li-ion batteries.

■ ASSOCIATED CONTENT

Supporting Information

The Supporting Information is available free of charge on the ACS Publications website at DOI: 10.1021/acssuschemeng.6b01032.

Experimental methods and characterization details; XRD of nontemplated LLZO; SEM, ligament size distribution, and XRD patterns for LLZO prepared using different calcination conditions; XRD patterns for NCF calcined in alumina vs quartz crucibles (PDF)

■ AUTHOR INFORMATION

Corresponding Author

*E-mail: candace.chan@asu.edu.

Notes

The authors declare no competing financial interest.

■ ACKNOWLEDGMENTS

This work was supported by NSF CAREER-1553519 and funding from the Fulton Undergraduate Research Initiative at ASU (Z.D.G.). We thank C. Wang and M. Li for assistance with performing the BET measurements. We also gratefully acknowledge the use of facilities within the LeRoy Center for Solid State Science and Goldwater Environmental Laboratory at ASU.

■ REFERENCES

(1) Tan, J.; Tiwari, A. Synthesis of Cubic Phase $Li_7La_3Zr_2O_{12}$ Electrolyte for Solid-State Lithium-Ion Batteries. *Electrochem. Solid-State Lett.* **2012**, *15* (3), A37.

(2) Murugan, R.; Thangadurai, V.; Weppner, W. Fast Lithium Ion Conduction in Garnet-Type $Li_7La_3Zr_2O_{12}$. *Angew. Chem., Int. Ed.* **2007**, *46* (41), 7778−7781.

DOI: 10.1021/acssuschemeng.6b01032
ACS Sustainable Chem. Eng. 2016, 4, 6391−6398

(3) Awaka, J.; Kijima, N.; Hayakawa, H.; Akimoto, J. Synthesis and Structure Analysis of Tetragonal $Li_7La_3Zr_2O_{12}$ with the Garnet-Related Type Structure. *J. Solid State Chem.* **2009**, *182* (8), 2046−2052.
(4) Geiger, C. A.; Alekseev, E.; Lazic, B.; Fisch, M.; Armbruster, T.; Langner, R.; Fechtelkord, M.; Kim, N.; Pettke, T.; Weppner, W. Crystal Chemistry and Stability of "$Li_7La_3Zr_2O_{12}$" garnet: A Fast Lithium-Ion Conductor. *Inorg. Chem.* **2011**, *50* (3), 1089−1097.
(5) Bernstein, N.; Johannes, M. D.; Hoang, K. Origin of the Structural Phase Transition in $Li_7La_3Zr_2O_{12}$. *Phys. Rev. Lett.* **2012**, *109* (20), 2−6.
(6) Logéat, A.; Köhler, T.; Eisele, U.; Stiaszny, B.; Harzer, A.; Tovar, M.; Senyshyn, A.; Ehrenberg, H.; Kozinsky, B. From Order to Disorder: The Structure of Lithium-Conducting Garnets $Li_{7-x}La_3Ta_xZr_{2-x}O_{12}$ (x = 0−2). *Solid State Ionics* **2012**, *206*, 33−38.
(7) Ohta, S.; Kobayashi, T.; Asaoka, T. High Lithium Ionic Conductivity in the Garnet-Type Oxide $Li_{7-X}La_3(Zr_{2-X},Nb_X)O_{12}$ (X = 0−2). *J. Power Sources* **2011**, *196* (6), 3342−3345.
(8) Wagner, R.; Redhammer, G. J.; Rettenwander, D.; Senyshyn, A.; Schmidt, W.; Wilkening, M.; Amthauer, G. Crystal Structure of Garnet-Related Li-Ion Conductor $Li_{7-3\,X}Ga_XLa_3Zr_2O_{12}$: Fast Li-Ion Conduction Caused by a Different Cubic Modification? *Chem. Mater.* **2016**, *28* (6), 1861−1871.
(9) Cheng, L.; Chen, W.; Kunz, M.; Persson, K.; Tamura, N.; Chen, G.; Doeff, M. Effect of Surface Microstructure on Electrochemical Performance of Garnet Solid Electrolytes. *ACS Appl. Mater. Interfaces* **2015**, *7* (3), 2073−2081.
(10) Matsui, M.; Takahashi, K.; Sakamoto, K.; Hirano, A.; Takeda, Y.; Yamamoto, O.; Imanishi, N. Phase Stability of a Garnet-Type Lithium Ion Conductor $Li_7La_3Zr_2O_{12}$. *Dalton Trans.* **2014**, *43* (3), 1019−1024.
(11) Yang, T.; Gordon, Z. D.; Li, Y.; Chan, C. K. Nanostructured Garnet-Type Solid Electrolytes for Lithium Batteries: Electrospinning Synthesis of $Li_7La_3Zr_2O_{12}$ Nanowires and Particle Size-Dependent Phase Transformation. *J. Phys. Chem. C* **2015**, *119* (27), 14947−14953.
(12) Boury, B.; Plumejeau, S. Metal Oxides and Polysaccharides: An Efficient Hybrid Association for Materials Chemistry. *Green Chem.* **2015**, *17* (1), 72−88.
(13) Schattka, J. H.; Wong, E. H.-M.; Antonietti, M.; Caruso, R. A. Sol−gel Templating of Membranes to Form Thick, Porous Titania, Titania/zirconia and Titania/silica Films. *J. Mater. Chem.* **2006**, *16* (15), 1414−1420.
(14) Greil, P. Templating Approaches Using Natural Cellular Plant Tissue. *MRS Bull.* **2010**, *35* (02), 145−149.
(15) Shigapov, A. N.; Graham, G. W.; McCabe, R. W.; Plummer, H. K. Preparation of High-Surface Area, Thermally-Stable, Metal-Oxide Catalysts and Supports by a Cellulose Templating Approach. *Appl. Catal., A* **2001**, *210* (1−2), 287−300.
(16) Huang, J.; Kunitake, T. Nano-Precision Replication of Natural Cellulosic Substances by Metal Oxides. *J. Am. Chem. Soc.* **2003**, *125* (39), 11834−11835.
(17) Stelte, W.; Sanadi, A. R. Preparation and Characterization of Cellulose Nanofibers from Two Commercial Hardwood and Softwood Pulps. *Ind. Eng. Chem. Res.* **2009**, *48* (24), 11211−11219.
(18) Gardner, D. J.; Oporto, G. S.; Mills, R.; Azizi Samir, M. A. S. Adhesion and Surface Issues in Cellulose and Nanocellulose. *J. Adhes. Sci. Technol.* **2008**, *22* (5−6), 545−567.
(19) Moon, R. J.; Martini, A.; Nairn, J.; Simonsen, J.; Youngblood, J. Cellulose Nanomaterials Review: Structure, Properties and Nanocomposites. *Chem. Soc. Rev.* **2011**, *40* (7), 3941.
(20) Peng, Y.; Gardner, D. J.; Han, Y.; Kiziltas, A.; Cai, Z.; Tshabalala, M. A. Influence of Drying Method on the Material Properties of Nanocellulose I: Thermostability and Crystallinity. *Cellulose* **2013**, *20* (5), 2379−2392.
(21) Wei, H.; Rodriguez, K.; Renneckar, S.; Vikesland, P. J. Environmental Science and Engineering Applications of Nanocellulose-Based Nanocomposites. *Environ. Sci.: Nano* **2014**, *1* (4), 302−316.
(22) Nair, S. S.; Zhu, J. Y.; Deng, Y.; Ragauskas, A. J. Hydrogels Prepared from Cross-Linked Nanofibrillated Cellulose. *ACS Sustainable Chem. Eng.* **2014**, *2* (4), 772−780.
(23) Zhang, Z.; Sèbe, G.; Rentsch, D.; Zimmermann, T.; Tingaut, P. Ultralightweight and Flexible Silylated Nanocellulose Sponges for the Selective Removal of Oil from Water. *Chem. Mater.* **2014**, *26* (8), 2659−2668.
(24) Zheng, Q.; Cai, Z.; Gong, S. Green Synthesis of Polyvinyl Alcohol (PVA)−cellulose Nanofibril (CNF) Hybrid Aerogels and Their Use as Superabsorbents. *J. Mater. Chem. A* **2014**, *2* (9), 3110.
(25) Dong, H.; Strawhecker, K. E.; Snyder, J. F.; Orlicki, J. A.; Reiner, R. S.; Rudie, A. W. Cellulose Nanocrystals as a Reinforcing Material for Electrospun Poly(methyl Methacrylate) Fibers: Formation, Properties and Nanomechanical Characterization. *Carbohydr. Polym.* **2012**, *87* (4), 2488−2495.
(26) Huang, J.; Zhu, H.; Chen, Y.; Preston, C.; Rohrbach, K.; Cumings, J.; Hu, L. Highly Transparent and Flexible Nanopaper Transistors. *ACS Nano* **2013**, *7* (3), 2106−2113.
(27) Janani, N.; Ramakumar, S.; Dhivya, L.; Deviannapoorani, C.; Saranya, K.; Murugan, R. Synthesis of Cubic $Li_7La_3Zr_2O_{12}$ by Modified Sol-Gel Process. *Ionics* **2011**, *17* (7), 575−580.
(28) Fleming, P.; Farrell, R. A.; Holmes, J. D.; Morris, M. A. The Rapid Formation of $La(OH)_3$ from La_2O_3 Powders on Exposure to Water Vapor. *J. Am. Ceram. Soc.* **2010**, *93* (4), 1187−1194.
(29) Kokal, I.; Somer, M.; Notten, P. H. L.; Hintzen, H. T. Sol−gel Synthesis and Lithium Ion Conductivity of $Li_7La_3Zr_2O_{12}$ with Garnet-Related Type Structure. *Solid State Ionics* **2011**, *185* (1), 42−46.
(30) Sakamoto, J.; Rangasamy, E.; Kim, H.; Kim, Y.; Wolfenstine, J. Synthesis of Nano-Scale Fast Ion Conducting Cubic $Li_7La_3Zr_2O_{12}$. *Nanotechnology* **2013**, *24* (42), 424005.
(31) Allen, J. L.; Wolfenstine, J.; Rangasamy, E.; Sakamoto, J. Effect of Substitution (Ta, Al, Ga) on the Conductivity of $Li_7La_3Zr_2O_{12}$. *J. Power Sources* **2012**, *206*, 315−319.
(32) Garvie, R. C. The Occurrence of Metastable Tetragonal Zirconia as a Crystallite Size Effect. *J. Phys. Chem.* **1965**, *69* (4), 1238−1243.
(33) Garvie, R. C. Stabilization of the Tetragonal Structure in Zirconia Microcrystals. *J. Phys. Chem.* **1978**, *82* (2), 218−224.
(34) Gribb, A. A.; Banfield, J. F. Particle Size Effects on Transformation Kinetics and Phase Stability in Nanocrystalline TiO_2. *Am. Mineral.* **1997**, *82*, 717−728.
(35) Hu, Y.; Tsai, H. L.; Huang, C. L. Phase Transformation of Precipitated TiO_2 Nanoparticles. *Mater. Sci. Eng., A* **2003**, *344* (1−2), 209−214.
(36) Zhang, H.; Banfield, J. F. Thermodynamic Analysis of Phase Stability of Nanocrystalline Titania. *J. Mater. Chem.* **1998**, *8* (9), 2073−2076.
(37) Chraska, T.; King, A. H.; Berndt, C. C. On the Size-Dependent Phase Transformation in Nanoparticulate Zirconia. *Mater. Sci. Eng., A* **2000**, *286* (1), 169−178.
(38) Baldinozzi, G.; Simeone, D.; Gosset, D.; Dutheil, M. Neutron Diffraction Study of the Size-Induced Tetragonal to Monoclinic Phase Transition in Zirconia Nanocrystals. *Phys. Rev. Lett.* **2003**, *90* (21), 216103.
(39) Cheng, L.; Chen, W.; Kunz, M.; Persson, K.; Tamura, N.; Chen, G.; Doeff, M. Effect of Surface Microstructure on Electrochemical Performance of Garnet Solid Electrolytes. *ACS Appl. Mater. Interfaces* **2015**, *7*, 2073−2081.
(40) Buschmann, H.; Dölle, J.; Berendts, S.; Kuhn, A.; Bottke, P.; Wilkening, M.; Heitjans, P.; Senyshyn, A.; Ehrenberg, H.; Lotnyk, A.; Duppel, V.; Kienle, L.; Janek, J. Structure and Dynamics of the Fast Lithium Ion Conductor "$Li_7La_3Zr_2O_{12}$. *Phys. Chem. Chem. Phys.* **2011**, *13*, 19378−19392.
(41) Kotobuki, M.; Munakata, H.; Kanamura, K.; Sato, Y.; Yoshida, T. Compatibility of $Li_7La_3Zr_2O_{12}$ Solid Electrolyte to All-Solid-State Battery Using Li Metal. *J. Electrochem. Soc.* **2010**, *157* (10), A1076−A1079.
(42) Chen, I.-W.; Wang, X.-H. Sintering Dense Nanocrystalline Ceramics without Final-Stage Grain Growth. *Nature* **2000**, *404*, 168−171.

DOI: 10.1021/acssuschemeng.6b01032
ACS Sustainable Chem. Eng. 2016, 4, 6391−6398

(43) Zhang, G.; Kirk, B.; Jauregui, L. A.; Yang, H.; Xu, X.; Chen, Y. P.; Wu, Y. Rational Synthesis of Ultrathin N-Type Bi_2Te_3 Nanowires with Enhanced Thermoelectric Properties. *Nano Lett.* **2012**, *12*, 56−60.
(44) Seabaugh, M. M.; Kerscht, I. H.; Messing, G. L. Texture Development by Templated Grain Growth in Liquid-Phase-Sintered Alpha-Alumina. *J. Am. Ceram. Soc.* **1997**, *80*, 1181−1188.
(45) Hou, Y.-D.; Hou, L.; Zhao, J.-L.; Zhu, M.-K.; Yan, H. Lead-Free Bi-Based Complex Perovskite Nanowires: Sol-Gel-Hydrothermal Processing and the Densification Behavior. *J. Electroceram.* **2011**, *26*, 37−43.
(46) Liu, W.; Liu, N.; Sun, J.; Hsu, P.-C.; Li, Y.; Lee, H.-W.; Cui, Y. Ionic Conductivity Enhancement of Polymer Electrolytes with Ceramic Nanowire Fillers. *Nano Lett.* **2015**, *15*, 2740−2745.
(47) Fu, K.; Gong, Y.; Dai, J.; Gong, A.; Han, X.; Yao, Y.; Wang, C.; Wang, Y.; Chen, Y.; Yan, C.; Li, Y.; Wachsman, E. D.; Hu, L. Flexible, Solid-State, Ion-Conducting Membrane with 3D Garnet Nanofiber Networks for Lithium Batteries. *Proc. Natl. Acad. Sci. U. S. A.* **2016**, *113*, 7094−7099.

DOI: 10.1021/acssuschemeng.6b01032
ACS Sustainable Chem. Eng. 2016, 4, 6391−6398